ELSEVIER

Journal of Nuclear Materials 296 (2001) 305–311

journal of nuclear materials

www.elsevier.com/locate/jnucmat

Section 6. Material engineering

Monitoring of low-cycle fatigue degradation in X6CrNiTi18-10 austenitic steel

M. Grosse *, M. Niffenegger, D. Kalkhof

Paul Scherrer Institut, CH-5232 Villigen, PSI, Switzerland

Abstract

The microstructural changes in the pre-crack stage of low-cycle fatigue damage (LCF) in austenitic piping steels were investigated by neutron and X-ray diffraction (XRD). The LCF damage evolution in the metastable austenitic steel causes a deformation-induced phase transformation from austenite to martensite. Thresholds exist for the formation of martensite as a function of accumulated plastic strain. Magnetic stray field and eddy current measurements were chosen to transfer the results of material characterisation to NDT methods. The density and distribution of martensite obtained by neutron diffraction experiments were used to adjust the NDT signals. Both NDT techniques were able to detect the very low amount of martensite in the different fatigued specimens (0.5–3.1 vol.% martensite) with usage factors from 0 up to 1.0. © 2001 Elsevier Science B.V. All rights reserved.

1. Introduction

The beam window of a pulsed spallation neutron source with liquid metal target is a new challenge for material research. Not only neutron and proton embrittlement, liquid metal erosion and corrosion but also thermal fatigue has to be taken into account. This problem is also relevant for continuous spallation sources. Typical beam trip rates of 30–50 per day result in loading cycle numbers in the order of magnitude of 10^4 per year. The knowledge about the interaction between fatigue degradation and irradiation hardening and embrittlement in a liquid metal environment is not satisfied. Experimental estimations of the fatigue behaviour under irradiation and liquid metal environment are extremely expensive and can only seldom be realised. Online or periodical non-destructive tests of the target window can contribute to a safe operation. In order to develop such test systems experiences of the monitoring of fatigue degradation in comparable materials can be used.

With regard to leaks in pressurised water pipes of nuclear power plants [1], which were caused by thermal fatigue damage, deformation-induced changes in the microstructure of metastable austenitic steel were investigated. It is well known that varying temperatures and thermal stratification in piping of power plants might cause fatigue damage by thermal strains. Such strains promote the phase transition from paramagnetic cubic face centred (fcc) austenite to ferromagnetic cubic body centred (bcc) martensite. This opens the possibility to detect the martensite content by means of magnetometers. In [2,3] this possibility is shown for duplex stainless steel and austenitic steel, respectively. Before these methods can be applied a better understanding of the influence of load parameters to the martensitic phase transition is needed.

Metallography as well as neutron and X-ray diffraction (XRD) are primarily intended to identify and quantify martensite formation in the pre-crack stage of low-cycle fatigue damage (LCF) in austenitic piping steels and its influencing parameters. To monitor the fatigue degradation, the application of magnetic NDT methods based on magnetic stray field and eddy current measurements is under investigation.

2. Materials and test conditions

Investigations were performed on hour-glass specimens (according to ASTM E606, Fig. 1). The material

* Corresponding author. Tel.: +41-56 310 2113; fax: +41-56 310 2199.

E-mail address: mirco.grosse@psi.ch (M. Grosse).

0022-3115/01/$ - see front matter © 2001 Elsevier Science B.V. All rights reserved.
PII: S0022-3115(01)00547-5

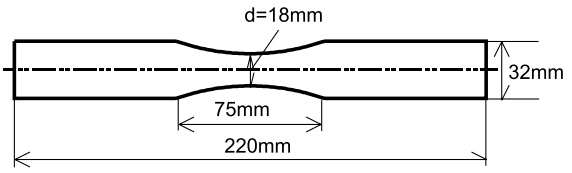

Fig. 1. Hour-glass specimens (ASTM E606).

under investigation was the titanium stabilised austenitic metastable steel X6CrNiTi18-10, which is widely used for vessels and piping. The chemical composition (in wt%) is given in Table 1. In order to homogenise the microstructure, the specimens were annealed at 1040°C (1 h) and afterwards quenched in oil. The total strain-controlled fatigue tests were performed with alternating loading and a test frequency of 2 s^{-1} at room temperature. A strain amplitude of $\pm 0.28\%$ for a gauge length of 25 mm was applied. Due to the shape of the sample the local strain depends on the axial position. Fig. 2 gives the results from FEM calculations of the distribution of plastic and total strains in the hour-glass specimen. The highest total strain amplitude is 0.60% at the position of the smallest cross-section. Plastic strains were evaluated up to an axial distance of ± 10 mm from the middle of the specimen. Different usage factors were realised by well-defined cycles of strain loads in series of hour-glass specimens.

Table 2 gives the cycle number for some investigated specimens and the corresponding usage factor D. The usage factor indicates how much lifetime is passed for a certain strain amplitude. D is defined to be equal to 1 for specimens, where crack initiation has occurred

Table 1
Chemical composition in wt% of the X6CrNiTi18-10 specimens (Fe-balance)

C	Mn	P	S	Cr	Ni	Ti
0.05	1.08	0.039	0.019	17.55	9.86	0.39

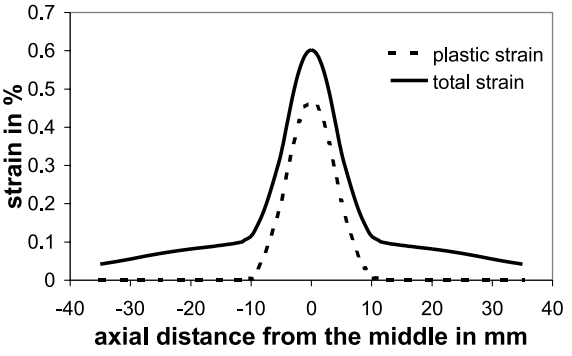

Fig. 2. Strain distribution along centre line in the hour-glass specimen.

(5% force drop). Therefore the corresponding cycle numbers vary for specimens with $D = 1$ due to differences in the damage progression. For specimens without a crack, D is defined as the ratio of the applied cycle number to an average cycle number representing crack initiation.

For the metallographic investigations, the specimens were cut in axial direction. After mechanical grinding and polishing, the specimens were etched with Beraha-II solution [4] to visualise the martensite. This etching results in a good contrast between martensite and austenite.

3. Structure investigations

3.1. Metallography

The metallographic investigations were performed on sample 1.6. Fig. 3 shows the microstructure at three axial positions. At positions close to the middle of the sample dark streaks were found. With increasing distances from the middle of the specimen the width of the streaks decreases down to zero. At positions far from the middle, the microstructure is homogeneous. The dark streak regions consist of martensite needles in an austenitic matrix (Fig. 4(a)). Outside these streaks only austenite grains were found (Fig. 4(b)).

3.2. Neutron diffraction

The martensite content formed by phase changes was measured by means of neutron and XRD. Austenite and martensite differ in their crystal structure. This makes it possible to determine the phase composition in the steel by neutron and XRD experiments.

Neglecting textures, the volume fraction of martensite x in the two-phase system (austenite and martensite) is given by [5]

$$x = [(I_{\{h,k,l\}_{\text{austenite}}}/I_{(h,k,l)_{\text{martensite}}})\ K_{1,2} + 1]^{-1}, \quad (1)$$

where $I_{\{h,k,l\}}$ is the intensity scattered at the lattice plane $\{h,k,l\}$, $K_{1,2}$ is a factor which considers the different structure types of martensite and austenite and the different angular positions of the reflexions, $K_{1,2}$ factors are tabulated for X-rays in [5] and can be calculated for neutrons [6]. A texture in the material cannot be excluded. Due to the one-dimensional loading a fiber texture of the strain-induced martensite can be expected. However, for a homogeneous texture of the martensite the estimated martensite content differs from the real content by a constant factor. The relative information used for the adjustment of the NDT methods is not affected by this problem.

Table 2
Martensite content obtained by neutron diffraction

Sample no.	Cycle number	Usage factor D	Crack position	Martensite (vol.%)
1.2	0	0	–	<0.50
2.4	0	0	–	<0.50
1.8	11200	0.4	–	<0.50
1.4	15850	0.6	–	0.61
2.2	15850	0.6	–	0.54
1.3	22400	0.8	–	0.95
1.7	22400	0.8	–	0.93
2.5	26000	1.0	5 mm away from the middle	1.49
2.3	32000	1.0	in the middle	1.49
1.6	63200	1.0	in the middle	3.13

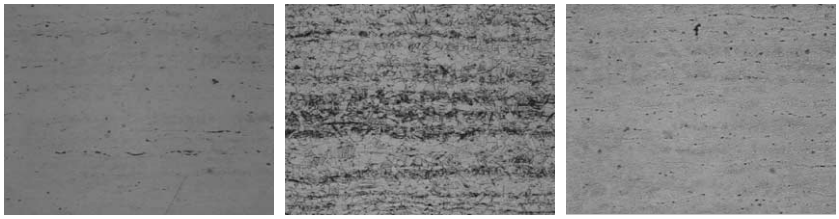

Fig. 3. Microstructure of specimen 1.6 at different axial positions.

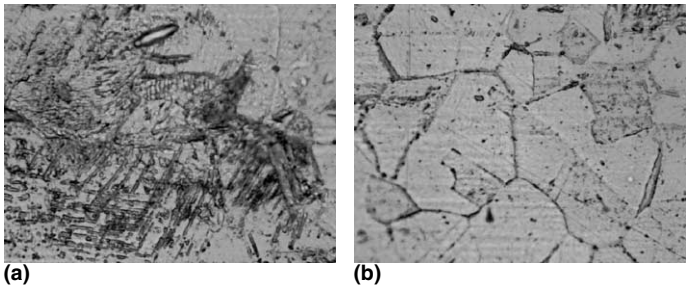

Fig. 4. Microstructure in the middle of specimen 1.6: (a) inside the streaks, (b) outside the streaks.

The neutron diffraction experiments were performed at the powder diffractometer DMC at the Swiss Spallation Neutron Source (SINQ). With a neutron beam wavelength of $\lambda = 0.38$ nm, a range of the scattering angle 2Θ of $68° \leqslant 2\Theta \leqslant 147°$ was analysed. Measurements on the vertically positioned LCF specimens were performed with a beam cross section of 40 mm (width) $\times$ 10 mm (height). The measuring position of these bulk measurements was in the middle of the LCF specimens ($\pm$5 mm in axial direction).

Results of martensite content x obtained by the bulk measurements are summarised in Table 2.

For LCF the well-known Coffin–Manson relation [7]

$$N_f^n \cdot \Delta\varepsilon_{a,p} = \text{const.} \tag{2}$$

describes the relation between the fracture cycle number N_f and the plastic strain amplitude $\Delta\varepsilon_{a,p}$. For steels the exponent n covers a range from 0.5 to 0.7. On this basis a parameter A shall be introduced with

$$A = N^n \, \Delta\varepsilon_{a,p}, \tag{3}$$

where N is the actual cycle number, A is a measure for the accumulated plastic strain. In order to describe the correlation between martensite content and accumulated plastic strain an exponent $n = 0.5$ gives the best results.

In Fig. 5 the martensite content x is plotted as a function of A for the results of the bulk measurements (diamonds, eps = 0.356%, N variable). Below a threshold value of $A \approx 0.35$ no martensite was obtained by neutron diffraction (detection limit is about 0.5 vol.%).

It shows that for starting the martensitic transformation a minimum of accumulated plastic strain is needed. At higher strains a linear dependence of the

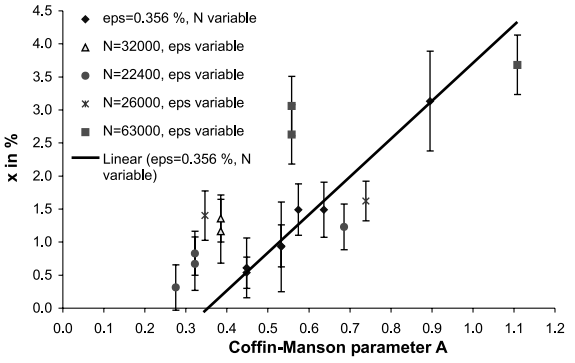

Fig. 5. Dependence of martensite content x on the accumulated plastic strain.

martensite content on the parameter A is found. Due to the hour-glass shape the local strain amplitude depends on the axial sample position. It allows to analyse the strain dependence of the martensitic transformation by local measurements of the martensite content with a reduced beam height of 2 mm. Fig. 6 shows the local distributions of the martensite for four specimens. Three of them, samples 1.6, 2.3 and 2.5 have $D = 1$. The maxima of the martensite content are detected at the crack position also in the case that the crack occurs not at the position with the smallest diameter. It seems that the crack formation results in an additional martensitic transformation. In the specimen 1.7 (without crack) the maximum of the martensite content was found at the smallest cross section. The martensite distribution in axial direction is non-symmetric for this specimen.

For the different axial positions the A parameter was calculated using the FEM results of strain distribution and the obtained data points are added in Fig. 5. The values obtained at positions where a crack was observed are excluded. The linear dependence of the martensite content on the A parameter found for the results of the bulk measurements is also valid for the results of the local measurement but the deviations of the data points from the fitted line are higher. A non-homogeneous texture which is strong at the beginning of the martensite formation and decreases with increasing martensite content can explain this higher deviations. However, it proves the linear dependence of the martensite content on the accumulated plastic strain described by the A parameter.

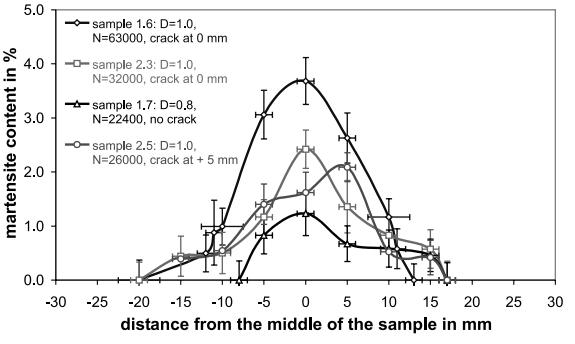

Fig. 6. Axial distribution of the martensite content for specimens 1.6, 1.7, 2.3 and 2.5.

3.3. X-ray diffraction (XRD)

Using synchrotron light sources the X-ray intensity is very high. This enables diffraction experiments with higher lateral resolution and shorter measurement periods than for neutron diffraction. Martensite distribution can be analysed in two dimensions at the sample surface. The experiments on specimen 1.6 were performed at the ROBL beamline at ESRF Grenoble (France) [8]. In order to use the $K_{1,2}$ values from [5], the wavelength of the Mo–Kα radiation ($\lambda = 0.07107$ nm) was applied. The investigated specimen was cut into two halves parallel to the sample axis. A mapping of the axial and radial martensite distribution was obtained by scanning the specimen through the fixed beam. With the applied wavelength and the beam cross section of 0.2 mm $\times$ 0.5 mm the gauge volume was about 1 mm (axial) $\times$ 0.5 mm (radial) $\times$ 0.005 mm (in depth). Fig. 7 shows the plastic zone estimated by the FEM calculations. As Fig. 8 shows the distribution of the martensite determined from the XRD data correlates with the shape of the plastic zone. In agreement with the ND measurements, in the axial direction, the martensite is found at the smallest cross section of the specimen according to the concentration of the plastic strain. In the radial direction, the martensite content is concentrated near the surface ($y = -6$ and 7 mm) and, as a broad area, in the centre of the specimen ($x, y = 0$ mm). The highest portion of martensite was found at the crack tip position. It confirms that the crack formation and growth is accompanied with an additional martensitic transformation.

However, outside the plastic zone no martensite was found.

4. Testing for LCF degradation by means of magnetic NDT methods

4.1. Measurements of magnetic stray field strength

After magnetising the specimens, the remanent field strength can be measured. The magnetisation of the specimens was carried out in a field with a strength of about 11 kA/m. Afterwards all specimens were examined using high sensitive fluxgate sensors. Measurements of the axial and normal components of the magnetic stray

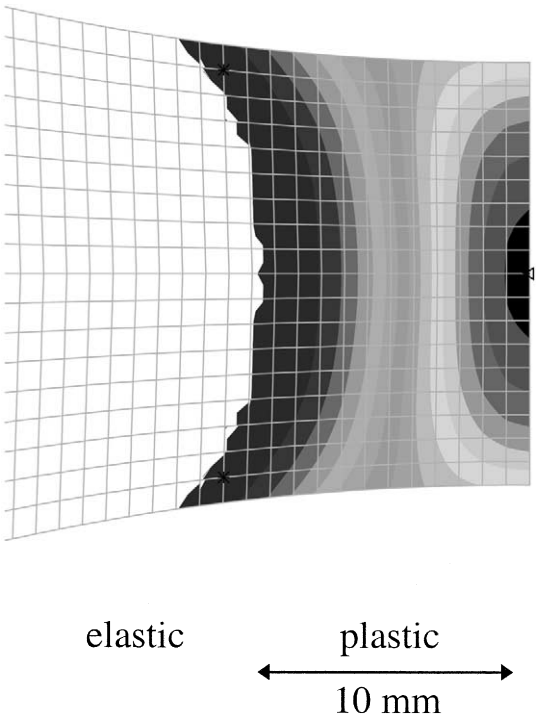

Fig. 7. FEM calculation of the plastic zone in the hour-glass specimen.

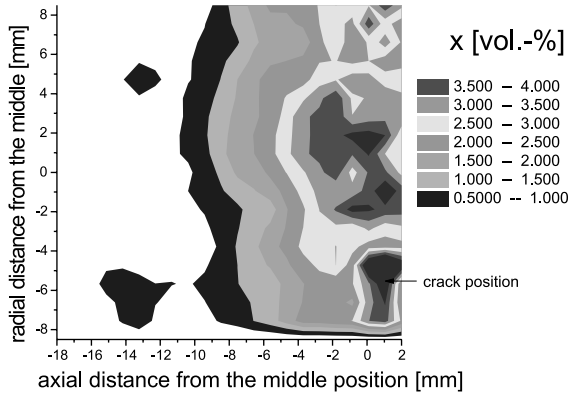

Fig. 8. Mapping of the radial and axial distribution of the martensite content.

field were performed in a distance of 20 mm from the bar axis. The fluxgate sensor was sensitive enough to detect the martensite areas. In Fig. 9 the fluxgate output (axial component) is plotted as a function of the axial scanning position. This output shows a pronounced positive peak when the sensor is directly over the position of the smallest cross section of the LCF samples. In the case of measurements on samples with crack ($D = 1$), the amplitude of field strength depends on the cycle number.

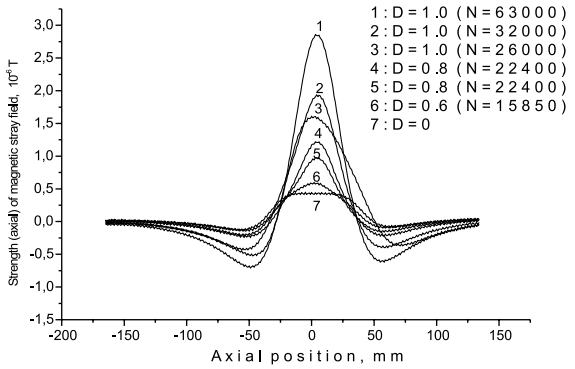

Fig. 9. Stray field measurements (fluxgate output) on LCF specimens of different usage factors, cycle numbers and martensite content.

For the pre-crack stages the amplitude of the fluxgate output increases with the usage factor. The LCF damage in the specimens can be detected down to the usage factor $D = 0.6$. At lower D the fluxgate output does not differ significantly. Also for the non-fatigued material a weak signal is detected. The reason for this is not yet clear. Very small amount of the ferromagnetic phases martensite and δ-ferrite (below the detection limit of the neutron and XRD) cannot be excluded.

4.2. Measurements by means of eddy current techniques

Eddy current techniques seem to be very promising for detecting LCF degradation. If the eddy current field is disturbed locally by changes of permeability, the eddy current signal is changed. The induced voltage amplitude with reference to a defined phase angle of the receiving coil was recorded. The manipulator system applied was able to follow the hour-glass shape of the specimens in a distance between sensor and surface of 1mm. For martensite visualisation a frequency of 50 kHz was used which provides a reasonable balance between high local resolution and depth of the eddy current field in the steel. For our measurements the penetration depth was about 2 mm. The lower and upper bounds of 0.5 and 3.15 vol.% martensite content defined the adjustment of the eddy current sensitivity.

For eddy current measurements, the end pieces of the LCF specimens were cut off and only the middle sections were used. Some examples of eddy current measurements performed at the circumferencial surface are plotted in Fig. 10. The axial specimen direction corresponds to the abscissa, the circumferential specimen directions (Φ-angle) correspond to the ordinate. Plots are shown for specimens with different usage factors (1.4, 1.7 and 2.3 with $D = 0.6$, 0.8 and 1.0, respectively). The martensite content of 0.61 vol.% for specimen 1.4 was clearly detected. The martensite is homogeneously

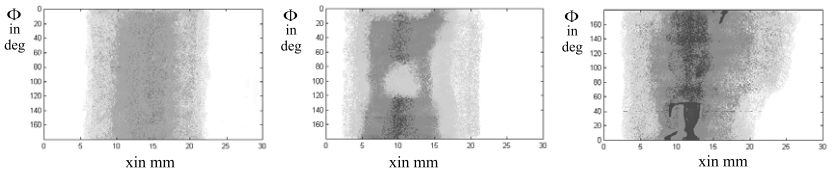

Fig. 10. Eddy current measurements on the circumferencial surface of LCF specimens: (a) sample 1.4 $D = 0.6, x_M = 0.61$ vol.%, (b) sample 1.7 $D = 0.8, x_M = 0.93$ vol.%, (c) sample 2.3 $D = 1.0, x_M = 1.49$ vol.%.

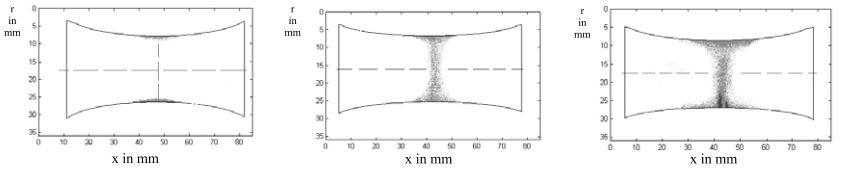

Fig. 11. Eddy current measurements on the axial cross-section of LCF specimens: (a) sample 1.4 $D = 0.6, x_M = 0.61$ vol.%, (b) sample 1.7 $D = 0.8, x_M = 0.93$ vol.%, (c) sample 2.3 $D = 1.0, x_M = 1.49$ vol.%.

distributed in the circumferential direction. The plot shows the beginning of the martensite formation during LCF loading. In the following damage stages $D = 0.8$ and $D = 1.0$, the martensitic pattern is the darker the more the usage factor increases. For specimen 1.7, the martensite is not as homogeneously distributed as for specimen 1.4. It agrees with the results of neutron scattering investigations. It is possible that the axial loading was accompanied by a small amount of bending. For specimen 2.3, loaded up to crack initiation, a single large crack was detected at the position of the smallest cross section. Furthermore, some local areas with a very high martensite concentration were found. These are probably new sources for macroscopic cracks. The martensite is homogeneously distributed. At the crack position an additional formation of martensite was observed.

Additionally, the specimens were cut in axial direction into two halves. Thus it was possible to determine the martensite distribution also in the radial specimen direction and obtain information about the progress of the martensite formation. In Fig. 11, the eddy current amplitudes at the axial cross section surface are plotted. The sensor output for specimen 1.4 shows that the formation of martensite is limited to the surface at the position of the smallest cross section. No martensite was detected in the bulk.

For further damage progression (specimen 1.7), the martensite tends to spread in depth. The axial distribution of martensite is wider at the surface than in the bulk. It seems that macroscopic crack initiation affects stress relaxation around this location. This results in a decrease of the martensite spreading in this area which is shown for specimen 2.3. The shape of the martensitic pattern is broader at the opposite side of the crack. axial cross section of LCF specimens.

5. Conclusions

All applied methods (neutron and XRD, magnetic stray field measurements with SQUID and fluxgate sensors, eddy current measurement) allowed the detection of martensite. While the amount of martensite is quantified with the diffraction methods, the magnetic techniques yield only relative results; that means, they have to be calibrated somehow, i.e. with results from neutron diffraction experiments.

It was shown that the content of martensite depends on the accumulated plastic strain and therefore on the usage factor. The existence of a threshold for the accumulated plastic strain to form deformation-induced martensite was demonstrated. This threshold is useful when examining industrial components under service conditions. The dependence of the threshold on other conditions of loading and temperature should be investigated in detail.

For our testing conditions both the eddy current technique as well as the stray field measurements were able to detect LCF damage down to $D = 0.6$. No significant differences of measuring signals for both techniques were found for $D < 0.6$, which corresponds to the results obtained by neutron diffraction experiments.

Acknowledgements

The authors thank Dr L. Keller (PSI) and Dr N. Schell (Forschungszentrum Rossendorf) for their support in the neutron and XRD experiments. We also are grateful to Dr J. Krause (FZ Jülich) and Professor D. Stegemann (Uni. Hanover) for their help in the magnetic

remanence field and eddy current measurements, repectively. This work was supported by the Swiss Federal Nuclear Safety Inspectorate, HSK.

References

[1] Experience with thermal fatigue in LWR piping caused by thermal mixing and stratification, OECD Nuclear Energy Agency, Paris, 1998; OECD NEA CSNI R(98)8.
[2] M. Otaka, S. Evanson, K. Hasegawa, K. Takaku, SMIRT 11 Transactions L (1991) 459.
[3] H.-J. Bassler, D. Eifler, in: K.T. Rie, P.D. Portella (Eds.), Low Cycle Fatigue and Elasto-Plastic Behaviour of Materials, Elsevier, Amsterdam, 1998, p. 285.
[4] E. Weck, E. Leistner, Metallographische Anleitung zum Farbätzen nach dem Tauchverfahren, Band2: Farbätzung nach Beraha und ihre Anwendungen, Deutscher Verlag für Schweisstechnik, Düsseldorf, 1983.
[5] G. Fanninger, U. Hartmann, Härterei Technische Mitteilungen HTM 27 (1972) 233.
[6] G.E. Bacon, Neutron Diffraction, Clarendon, Oxford, 1975.
[7] G. Schott, Werkstoffermüdung – Ermüdungsfestigkeit, Deutscher Verlag für Grundstoffindustrie, Stuttgart, 1997.
[8] W. Matz et al., J. Synchron. Rad. 6 (1999) 1076.